

LORENTZ ANGLE STUDIES FOR THE SLD ENDCAP
ČERENKOV RING IMAGING DETECTOR *

P. COYLE, M. CAVALLI-SFORZA, D. COYNE,
M. SCHNEIDER, E. SPENCER, D. WILLIAMS

University of California, Santa Cruz, CA 95064

V. ASHFORD¹, T. BIENZ, F. BIRD, M. GAILLARD², G. HALLEWELL,
Y.J. KWON, D. LEITH, D. MCSHURLEY, A. NUTTALL, G. OXOBY,
H. PETERSON, B. RATCLIFF, R. REIF, P. RENSING, D. SCHULTZ,
R. SHAW, S. SHAPIRO, N. TOGE, J. VA'VRA, T. WEBER, S. WILLIAMS³

Stanford Linear Accelerator Center, P.O. Box 4349, Stanford, CA 94305

D. BAUER, D. CALDWELL, D. HALE, A. LU, S. YELLIN

University of California, Santa Barbara, CA 93106

R. JOHNSON, B. MEADOWS, M. NUSSBAUM

University of Cincinnati, Cincinnati, OH 45221

ABSTRACT

The design of the endcap Čerenkov Ring Imaging Detectors for SLD requires a detailed understanding of how electrons drift in gases under the influence of crossed electric and magnetic fields. In this report, we present recent measurements of Lorentz angles and drift velocities in gases suitable for the endcap CRID photon detectors. We compare these measurements to predictions from a theoretical model; good agreement is observed. Based on our results we present a design for detectors operating in a 0.6 Tesla transverse magnetic field.

*Poster Presentation at the London Conference on Position Sensitive Detectors
September 7 - 11, 1987, University College London, England*

* Work supported by the Department of Energy, contracts DE-AC03-76SF00515 and DE-AT03-79ER70023 and by the National Science Foundation under Grants PHY85-12145 and PHY85-13808.

1 Present Address: University of California, San Diego, La Jolla, CA 92023.

2 Present Address: Lab. de l'Accelérateur Lineaire, Batiment 200, F91405 Orsay, Cedex, France

3 Present Address: Diconics Corporation, 533 Cabot Rd., South San Francisco, CA 94080

1. Introduction

The Čerenkov Ring Imaging Detectors (CRIDs) are an integral part of the powerful particle identification capability of the new detector, the SLD [1] (figure 1), being built for the SLAC Linear Collider (SLC). In the CRID (figure 2), relativistic charged particles

passing through liquid and gaseous freon radiators produce Čerenkov light at angles characteristic of the particle velocity. The Čerenkov light from the liquid radiator is proximity focused on one side of a quartz drift box; the light from the gaseous radiator is reflected by spherical mirrors and enters the drift box from the other side. The Čerenkov photons release electrons within the drift boxes by ionization of the photo-sensitive gas tetrakis (dimethylamino) ethylene (TMAE). These photoelectrons then drift in a uniform electric field and are detected by a proportional sense wire plane.

Two CRID systems are being built for the SLD: the barrel CRID [2], which will identify particles in the central region, and the endcap CRIDs, which will cover the forward and backward regions. The major difference between these two systems is the orientation of the drift electric field with respect to the 0.6 Tesla magnetic field of the SLD magnet. In the barrel, the electrons drift parallel to both the magnetic and electric fields. In the endcap the electrons drift perpendicular to the magnetic field and as a result drift at an angle, known as the Lorentz angle, relative to the electric field direction. As we will show in section 2, our endcap design relies on knowledge of the expected Lorentz angle. We report here on our recent experimental and theoretical studies of the dependence of the Lorentz angle upon the drift gas composition and the strengths of the electric and magnetic fields.

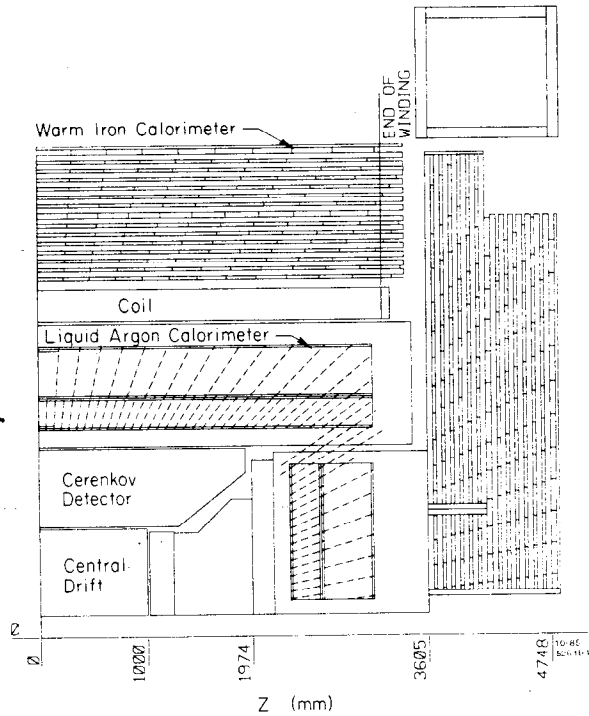


Fig. 1. One-quarter cross section of the SLD detector at SLC.

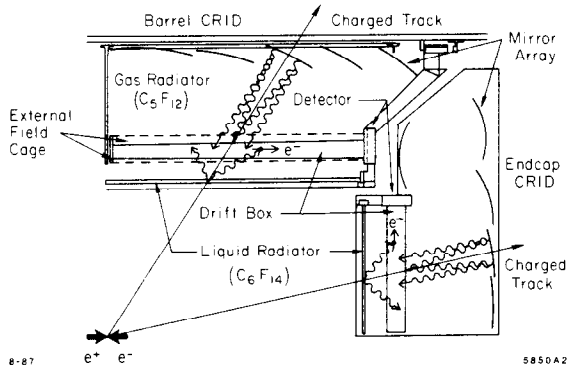


Fig. 2. Principle of operation of the barrel and endcap CRIDs.

2. Endcap Design Considerations

The endcap design we have adopted incorporates the sector type geometry shown in figure 3. For each mechanically separate sector, the inward electric field is generated by field defining wires on the quartz surfaces.

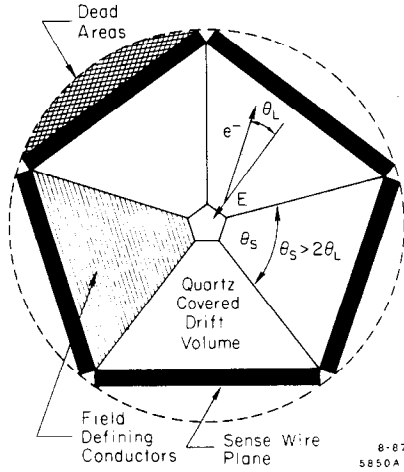


Fig. 3. A five sector endcap design. θ_L is the Lorentz angle; θ_S is the sector angle.

A major advantage of this configuration is that the sense planes, located near the circumference, are readily accessible. For this design it is preferable to have many sectors, since this reduces the area of the dead regions behind the sense planes, decreases the area of each drift box and shortens the length of the sense planes. The number of sectors attainable in practice is limited by the Lorentz angle in the gas. To collect all the ionization produced in a drift volume, the sector opening angle must be at least twice the Lorentz angle. Table 1 shows the maximum Lorentz angle and sense plane length for various sector counts. We see that a five sector geometry, which gives a sector angle of 72° , requires a Lorentz angle of less than 36° .

Table 1. Endcap parameters for various numbers of sectors.

Number of Sectors	Maximum Lorentz Angle (Degrees)	Sense Plane Length (cm)
4	45.0	88
5	36.0	73
6	30.0	63
8	22.5	48
10	18.0	38
12	15.0	32

The presence of the Lorentz angle also complicates the transfer of the electrons from the drift region to the sense planes [3]. Since TMAE is sensitive to photons produced in the electron avalanche, the solid angle available for these photons to reach the drift volume must be reduced (the anode wires must be blinded). Of course, this must be achieved while remaining fully efficient for electron detection. In the barrel CRID this is accomplished using a series of blinding grids in front of the sense wire plane, these focus

the photoelectrons towards the sense wires, while obstructing the paths of photons generated at the sense wires. Although this scheme is optimized to be 100% efficient for the detection of electrons in the absence of a magnetic field, inefficiency may arise in the presence of a perpendicular magnetic field; in this case, the Lorentz angle can cause electrons to be diverted to trajectories which terminate on the blinding grid rather than the sense wires. Although we have yet to choose the final design of the sense wire plane and blinding structure for the endcaps, our studies indicate that full efficiency is more easily obtained with smaller Lorentz angles.

In addition to a small Lorentz angle, the endcap CRID gas mixture must have good UV transmission over the photon wavelength range between 230 nm (the TMAE ionization threshold) and 165 nm (the quartz cut-off). Furthermore, it must quench the electron avalanche to prevent breakdown, while yielding sufficient gain for single electron detection. In order to achieve efficient drift over large drift lengths, the gas should have a long attenuation length for electron capture, and finally, it should have a small diffusion coefficient in order to maintain good spatial resolution. We have therefore limited our Lorentz angle measurements to gas mixtures composed of the following components: methane, ethane, isobutane, carbon dioxide and the inert gases. These are gases known to satisfy the majority of the requirements noted above.

3. Measuring the Lorentz Angle

The Lorentz angle measurements were performed using a small (20 cm × 20 cm × 5 cm) time projection chamber (TPC) placed in a spectrometer magnet (figure 4). Light from a nitrogen laser was piped along two quartz optical fibers and entered the drift volume through a quartz window which formed the front surface of the TPC. By measuring the differences in detected positions and arrival times of the electrons produced by each fiber, the Lorentz angle and drift velocity were determined.

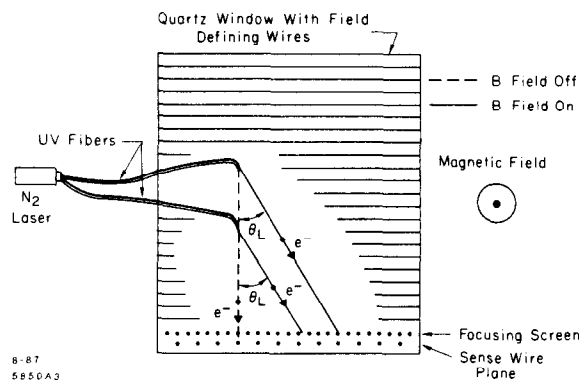


Fig. 4. Apparatus for measuring the Lorentz angle. The drift paths of the electrons with and without the magnetic field are indicated.

Due to the small size of our TPC, it was not always possible to measure the Lorentz angle at the SLD design value for the magnetic field. To extrapolate our measurements to a field of 0.6 Tesla we used the calculational technique described by Schultz [4]. This approach is based on the classical theory of electron transport phenomena originally developed by Morse et al. [5] and later extended by others [6-8].

In this model, the energy distribution of the electrons in a gas mixture is obtained from an approximate solution of the Boltzmann transport equation. The model takes into account the effect of elastic and inelastic collisions (resulting in rotational or vibration excitation) on the energy distribution of the electrons, but neglects effects due to electronic excitation and ionizing collisions. Magnetic field effects are taken into account using the procedure described by Ramanantsoahena et al. [9]. To numerically solve the integrodifferential equations involved in this model we have developed a computer program which evaluates the electron energy distribution in the specified gas mixture. This distribution is then used to calculate all the electron transport parameters, including the drift velocity and Lorentz angle, at any electric or magnetic field value.

The only data input to the program are the elastic and inelastic cross sections of the component gases. In practice, these are usually defined by tuning their assumed energy dependence until good agreement is found between the measured and calculated transport parameters. Having fixed the cross sections using data for one particular gas mixture, the model is then able to predict the transport parameters for an arbitrary mixture at any electric or magnetic field strength. For our calculations, we have not attempted to derive the cross sections, but have used values available in the literature for methane [4], ethane [10], isobutane [4], carbon dioxide [4], argon [4], and neon [11]. Where possible we have compared the results from our program with results from other similar programs [4,8,9,10,12]; in all cases excellent agreement was found.

Although neither our measurements nor our calculations include the effect of a TMAE component in the gas mixture, we expect its influence to be small due to its low concentration (~ 1000 ppm for 28°C TMAE). This assumption is justified since the addition of TMAE to a gas mixture does not modify appreciably the observed drift velocities [13].

4. Results and Discussion

Table 2 shows our measurements of the Lorentz angle and drift velocity for various isobutane/methane mixtures. Included in this table are the values for these two quantities predicted by our program. Figure 5 plots the Lorentz angle as a function of magnetic field for a selection of these data. We see an almost linear dependence of Lorentz angle on the magnetic field, a dependence which is well-reproduced by the model.

Table 3 shows similar measurements for ethane/methane mixtures and figure 6 plots the measured and predicted Lorentz angles and drift velocities for these data as function of the methane/ethane ratio. We see that methane and ethane have similar Lorentz angle characteristics.

Table 4 shows our measurements for various inert gas/quencher mixtures, while figure 7 plots some of the data for the 55% Neon/45% isobutane mixture.

Fig. 5. Lorentz angles and drift velocities for various isobutane-methane mixtures.

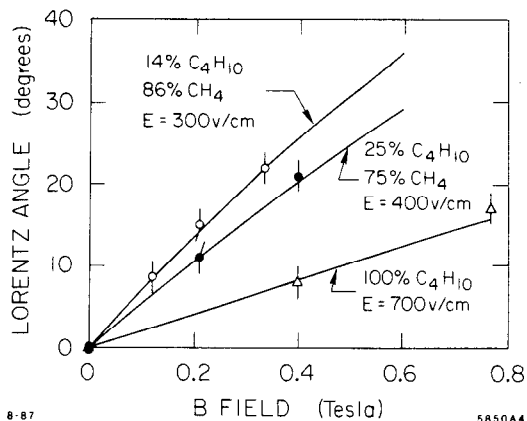


Table 2. Lorentz angles and drift velocities for various isobutane-methane mixtures.

Gas Mixture	B Field (Tesla)	E Field (V/cm)	Lorentz Angle (Degrees)		Drift Velocity (cm/ μ s)	
			Measured	Calculated	Measured	Calculated
100% Isobutane	0.0	250	—	—	0.8 \pm 0.3	0.9
		350	—	—	1.1 \pm 0.3	1.3
		550	—	—	1.9 \pm 0.3	2.0
		700	—	—	2.5 \pm 0.3	2.5
	0.4	250	7.0 \pm 2.0	8.5	0.7 \pm 0.3	0.9
		350	7.0 \pm 2.0	8.5	1.1 \pm 0.3	1.3
		550	8.0 \pm 2.0	8.4	1.9 \pm 0.3	2.0
		700	8.0 \pm 2.0	8.3	2.4 \pm 0.3	2.5
	0.77	250	16.0 \pm 2.0	16.1	0.8 \pm 0.3	0.9
		350	16.0 \pm 2.0	16.0	1.1 \pm 0.3	1.2
		550	17.0 \pm 2.0	15.9	1.8 \pm 0.3	1.9
		700	17.0 \pm 2.0	15.7	2.3 \pm 0.3	2.4
25% Isobutane 75% Methane	0.0	138	—	—	1.1 \pm 0.3	1.3
		200	—	—	1.7 \pm 0.3	1.9
		300	—	—	2.7 \pm 0.3	2.8
		400	—	—	3.9 \pm 0.3	3.7
	0.21	138	8.0 \pm 2.0	11.2	1.1 \pm 0.3	1.3
		200	11.0 \pm 2.0	11.2	1.7 \pm 0.3	1.8
		300	11.0 \pm 2.0	11.1	2.7 \pm 0.3	2.7
		400	11.0 \pm 2.0	11.0	3.6 \pm 0.3	3.6
	0.4	138	20.0 \pm 2.0	20.7	1.0 \pm 0.3	1.2
		200	22.0 \pm 2.0	20.7	1.6 \pm 0.3	1.8
		300	20.0 \pm 2.0	20.6	2.4 \pm 0.3	2.6
		400	21.0 \pm 2.0	20.3	3.5 \pm 0.3	3.5
14% Isobutane 86% Methane	0.0	200	—	—	2.3 \pm 0.3	2.4
		300	—	—	3.6 \pm 0.3	3.6
	0.12	200	9.0 \pm 2.0	8.3	2.4 \pm 0.3	2.4
		300	9.0 \pm 2.0	8.2	3.8 \pm 0.3	3.5
	0.21	200	15.0 \pm 2.0	14.3	2.3 \pm 0.3	2.3
		300	15.0 \pm 2.0	14.2	3.5 \pm 0.3	3.5
	0.335	200	24.0 \pm 2.0	22.2	2.1 \pm 0.3	2.2
		300	22.0 \pm 2.0	22.0	3.2 \pm 0.3	3.3

Fig. 6. Lorentz angles and drift velocities as a function of the ethane-methane mixture ratio.

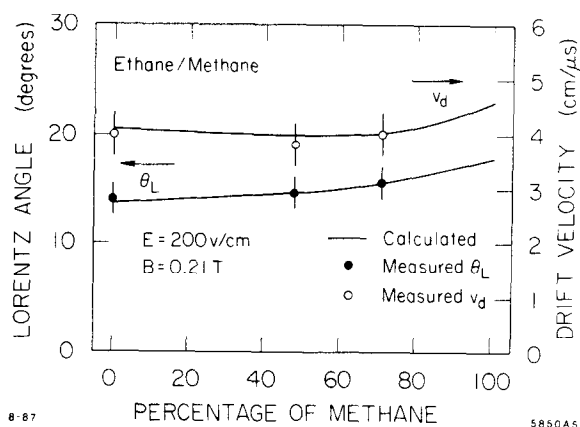


Table 3. Lorentz angles and drift velocities for various ethane-methane mixtures.

Gas Mixture	B Field (Tesla)	E Field (V/cm)	Lorentz Angle (Degrees)		Drift Velocity (cm/μs)	
			Measured	Calculated	Measured	Calculated
100% Methane	0	150	—	—	3.0 ± 0.3	2.87
	0.2	150	23.0 ± 2.0	21.1	2.7 ± 0.3	2.68
29% Ethane 71% Methane	0	125	—	—	2.0 ± 0.3	2.11
		200	—	—	3.3 ± 0.3	3.28
	0.21	125	21.0 ± 2.0	20.7	1.9 ± 0.3	1.97
		200	20.0 ± 2.0	20.1	3.1 ± 0.3	3.10
52% Ethane 48% Methane	0	200	—	—	3.2 ± 0.3	3.10
		250	—	—	3.6 ± 0.3	3.64
	0.21	200	19.0 ± 2.0	19.9	2.9 ± 0.3	2.92
		250	19.0 ± 2.0	19.1	3.3 ± 0.3	3.49
100% Ethane	0	75	—	—	1.2 ± 0.3	1.17
		150	—	—	2.3 ± 0.3	2.29
		200	—	—	3.1 ± 0.3	2.89
		250	—	—	3.4 ± 0.3	3.36
	0.21	75	22.0 ± 2.0	21.8	1.1 ± 0.3	1.09
		150	21.0 ± 2.0	21.2	2.1 ± 0.3	2.14
		200	20.0 ± 2.0	20.5	2.8 ± 0.3	2.74
		250	19.0 ± 2.0	19.5	3.4 ± 0.3	3.23

Fig. 7. Lorentz angles and drift velocities for a 55% neon/45% isobutane mixture.

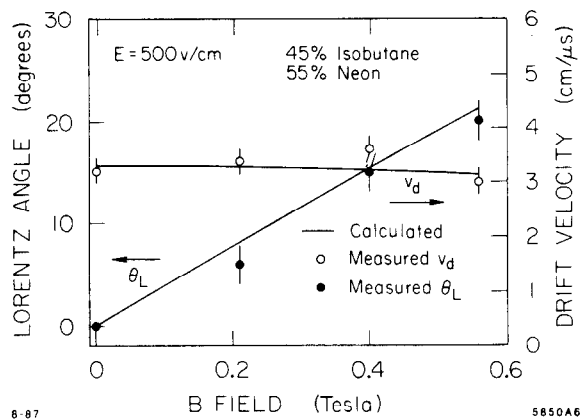


Table 4. Lorentz angles and drift velocities for various inert gas/quencher mixtures.

Gas Mixture	B Field (Tesla)	E Field (V/cm)	Lorentz Angle (Degrees)		Drift Velocity (cm/μs)	
			Measured	Calculated	Measured	Calculated
55% Neon 45% Isobutane	0.0	320	—	—	2.3 ± 0.3	2.34
		500	—	—	3.2 ± 0.3	3.31
		600	—	—	3.6 ± 0.3	3.71
		700	—	—	4.0 ± 0.3	4.03
	0.21	320	10.0 ± 2.0	8.9	2.3 ± 0.3	2.30
		500	6.0 ± 2.0	8.2	3.4 ± 0.3	3.25
		600	11.0 ± 2.0	7.8	4.0 ± 0.3	3.69
	0.275	700	10.0 ± 2.0	9.6	3.8 ± 0.3	4.00
	0.4	320	18.0 ± 2.0	16.6	2.2 ± 0.3	2.25
		500	15.0 ± 2.0	15.4	3.6 ± 0.3	3.22
		600	20.0 ± 2.0	14.7	4.0 ± 0.3	3.60
	0.56	320	23.0 ± 2.0	22.7	2.2 ± 0.3	2.18
		500	20.0 ± 2.0	21.2	3.0 ± 0.3	3.14
		600	20.0 ± 2.0	20.3	3.6 ± 0.3	3.56
		700	18.0 ± 2.0	19.3	3.7 ± 0.3	3.90
49% Neon 51% Ethane	0.0	250	—	—	3.9 ± 0.3	3.85
		350	—	—	4.3 ± 0.3	4.21
	0.21	250	18.0 ± 2.0	23.3	3.7 ± 0.3	3.73
		350	15.0 ± 2.0	19.2	4.2 ± 0.3	4.15
88% Argon 12% Isobutane	0.0	100	—	—	2.4 ± 0.3	2.25
		140	—	—	3.1 ± 0.3	3.14
	0.18	100	24.0 ± 2.0	22.0	2.1 ± 0.3	2.07
		140	21.0 ± 2.0	22.2	2.9 ± 0.3	2.93

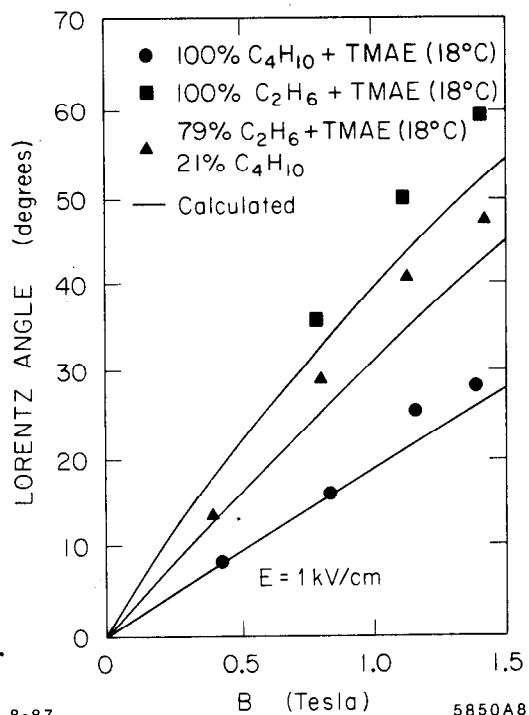


Fig. 8. Comparison of the program predictions with the measurements of W. Dulinski et al. [3].

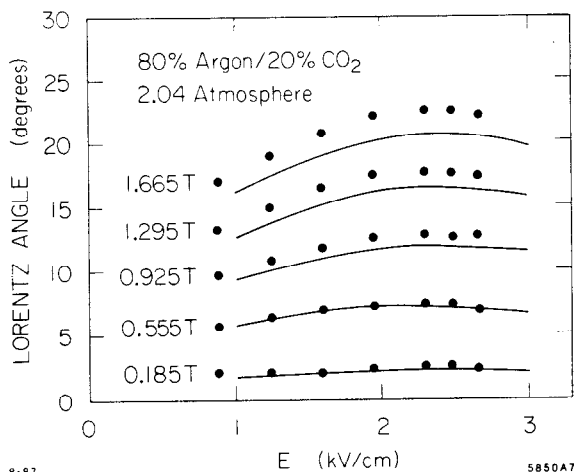
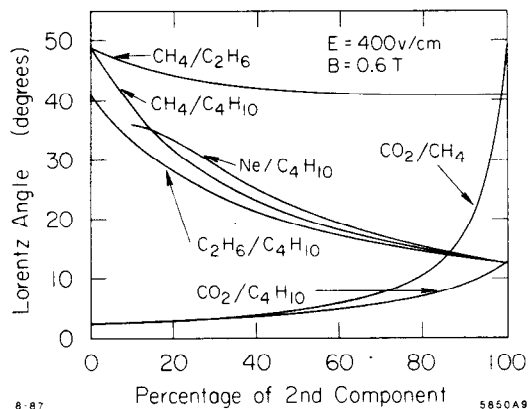


Fig. 9. Comparison of the program predictions with the measurements of C. Ma et al. [14].

In general, the agreement between the predictions of the model and our measurements is very good. As a further check of the program, we have compared its predictions to measurements by other groups. Figure 8 compares the model predictions with the measurements of Dulinski et al. [3] in ethane/isobutane/TMAE mixtures. We see reasonable agreement, although the ethane/TMAE predictions deviate significantly from the measurements at high magnetic field. Figure 9 compares the Lorentz angle predictions with measurements of C. Ma et al. [14] in argon/carbon dioxide mixtures at 2.04 atmospheres. The agreement between the model and the data is satisfactory at low magnetic fields, but again at higher fields the predictions from the model are lower by $\approx 10\%$.

The above comparisons indicate that the program yields reliable predictions, especially at the low magnetic fields of interest for SLD. We have therefore used the program to predict the Lorentz angles for a 0.6 Tesla magnetic field in various gas mixtures of interest. The results are shown in figure 10. For this plot we have assumed an electric field of 400 V/cm, the design value for the electric field in the Barrel CRID. From this plot we see that the mixture of methane/ethane, commonly used in ring imaging detectors, gives a Lorentz angle of $\approx 45^\circ$. This angle would restrict us to a four sector design. Due to large dead regions ($\approx 36\%$) and long sense planes (≈ 90 cm) this design is not acceptable. With appropriate mixtures of methane/isobutane or ethane/isobutane we can obtain Lorentz angles small enough for endcaps designs with up to ten sectors. The

Fig. 10. Calculated Lorentz angles at 0.6T for various gas mixtures.



addition of a small amount of carbon dioxide to methane, ethane or isobutane would allow us to have twelve or more sectors. As the transmission edge of carbon dioxide is at 180 nm, 15 nm beyond the quartz cut-off, its use would reduce the detector efficiency appreciably.

The endcap geometry of particular interest to us is a design consisting of ten sectors. This configuration matches the ten-fold symmetry used in the barrel CRID and yields sense planes of manageable length (≈ 40 cm). A ten sector design requires a gas mixture with a Lorentz angle less than 18° and therefore dictates the use of gas mixtures with a large isobutane component or a small carbon dioxide component. Before committing ourselves to a final choice of gas mixture and sector count, further work is necessary to investigate in detail the other important gas properties required of the endcap CRID gas (e.g. pulse height spectra, electron absorption length, UV absorption, diffusion, etc.). These studies are in progress for the smaller Lorentz angle gases we have examined.

REFERENCES

1. M. Breidenbach, *et al.*, IEEE Trans. Nucl. Sci. NS33 (1986) 46.
2. V. Ashford *et al.*, IEEE Trans. Nucl. Sci. NS54 (1986) 98.
3. W. Dulinski *et al.*, Nucl. Instr. Meth. A252 (1986) 418.
4. G. Schultz and J. Gresser, Nucl. Instr. Meth. 151 (1978) 413.
5. P. M. Morse, W. P. Allis and E. S. Lamar, Phys. Rev. 48 (1935) 412.
6. T. Holstein, Phys. Rev. 70 (1946) 367.
7. L. S. Frost and A. V. Phelps, Phys. Rev. 127 (1962) 1621.
8. V. Palladino and B. Sadoulet, Nucl. Instr. Meth. 128 (1975) 323.
9. P. Ramanantsizehena, J. Gresser and G. Schultz, Nucl. Instr. Meth. 178 (1980) 253.
10. Y. Chatelus, P. Ramanantsizehena, J. Gresser and G. Schultz, Nucl. Instr. Meth. 171 (1980) 127.
11. L. Huxley and R. Crompton, *The Diffusion and Drift of Electrons In Gases*, John Wiley & Sons (1974) 607.
12. U. Becker *et al.*, Nucl. Instr. Meth. 214 (1983) 525.
13. G. Charpak and F. Sauli, Nucl. Instr. Meth. 225 (1984) 627.
14. C. Ma *et al.*, MIT Technical Report (1982) 129.